Very low frequency earthquakes within accretionary prisms are very low stress-drop earthquakes

doi: 10.1029/2006GL025883

Very low frequency earthquakes within accretionary prisms are very low stress-drop earthquakes

Yoshihiro Ito[1] and Kazushige Obara[1]

Received 27 January 2006; revised 14 March 2006; accepted 24 March 2006; published 4 May 2006.

[1] We report characteristic *P* wave spectra and stress drops of very low frequency (VLF) earthquakes that occurred within the accretionary prism along the Nankai Trough, southwestern Japan. Although many VLF earthquakes showed no distinct phases on a raw seismogram, a few showed slightly distinct phases. The arrival times of some phases were consistent with the calculated *P* wave arrival times. The corner frequencies of the VLF earthquakes were calculated using the stacked *P* wave spectra assuming an omega-square spectrum. Stress drops were very low, i.e., in the range of 0.1–10 kPa, which corresponds to 0.1%–1% of those of ordinary earthquakes. Such extremely low stress drops of the VLF earthquakes suggest that the fault strength within the accretionary prism may have weakened due to the existence of a fluid within the thrust fault system of the accretionary prism. **Citation:** Ito, Y., and K. Obara (2006), Very low frequency earthquakes within accretionary prisms are very low stress-drop earthquakes, *Geophys. Res. Lett.*, *33*, L09302, doi:10.1029/2006GL025883.

1. Introduction

[2] Megathrust earthquakes occur repeatedly along the Nankai Trough, southwestern Japan, and they are associated with the subduction of the Philippine Sea Plate beneath the margin of the Eurasian Plate at a rate of ~4 cm/yr [*Seno et al.*, 1993]. Recently, some types of slow earthquakes have been detected along the Nankai Trough [e.g., *Obara*, 2002; *Obara et al.*, 2004; *Obara and Ito*, 2005; *Ito and Obara*, 2006]. *Obara* [2002] discovered a non-volcanic deep tremor within the crust at a depth of 30 km along the Nankai Trough beneath southwestern Japan. This phenomenon couples with the slow slip events occurring around the sources of tremors [*Obara et al.*, 2004]. In order to reveal the megathrust earthquake cycle, it is important to understand these slow events.

[3] Very low frequency (VLF) earthquakes, which are a type of slow earthquakes, within the accretionary prism have been detected near the trench axis along the Nankai Trough [*Obara and Ito*, 2005; *Ito and Obara*, 2006]. These earthquakes have not been described in any earthquake catalog because they have no distinct short period phases of the *P* or *S* wave component. The VLF earthquakes along the Nankai Trough can be studied using a frequency window between 10–20 s [*Obara and Ito*, 2005]. Low-frequency wave trains are composed of surface waves with an apparent velocity of around 3.5–4.0 km/s; further, earthquake epicenters are located landward of the Nankai Trough, as estimated from the directions of the wave train propagation [*Obara and Ito*, 2005]. Their source depths are distributed within the accretionary prism above the plate boundary between the Philippine Sea Plate and Eurasian Plate and within a distance of 50–70 km landward of the trough axis; they exhibit reverse faulting, suggesting the dynamic deformation of the accretionary prism [*Ito and Obara*, 2006]. However, the rupture process of these VLF earthquakes has never been discussed.

[4] First, we investigate the waveforms and detect the phases of *P* waves of VLF earthquakes. Next, we calculate the Fourier spectrum of these *P* waves. Finally, we estimate the corner frequencies and stress drops, which provide important information on the source process of an earthquake. Finally, we discuss the relationship between the fault size and slip of the VLF earthquakes within the accretionary prism.

2. Data

[5] We used the hypocenters of the VLF earthquakes obtained by *Ito and Obara* [2006] (Figure 1b). The centroid locations, centroid times, and moment tensor solutions of 18 VLF earthquakes occurring off the Kii peninsula along the Nankai Trough are calculated by the centroid moment tensor inversion method.

[6] Seismograms observed using the NIED broadband velocity seismometer network (NIED F-net) were used (Figure 1a). Three-component broadband velocity seismometers (STS-1/2) were installed at each F-net station in a tunnel and spaced 100 km apart [*Okada et al.*, 2004]. The seismic data from each F-net station were digitized using 24 bit A/D converters. The original data with a sampling frequency of 1 KHz was decimated to a sampling frequency of 100 Hz. The data observed at each station were deconvolved with the instrumental responses of the seismometers and digitizers.

3. Detection and Spectrum of *P* Wave

[7] We investigated the seismogram of the vertical component. Although most of the observed waveforms of the VLF earthquakes that were filtered with a wide pass band of 0.005–20 Hz showed no phases (Figure 2a), those filtered with a pass band of 0.01–0.1 Hz showed the distinct large phases of surface waves. Furthermore, slightly distinct phases were detected before the arrival of surface waves on seismograms filtered with a pass band of 0.01–0.1 Hz. The arrival times of these phases were consistent with the *P* wave or *S* wave travel times calculated on the basis of the

[1]National Research Institute for Earth Science and Disaster Prevention, Tsukuba, Japan.

0094-8276/06/2006GL025883$05.00

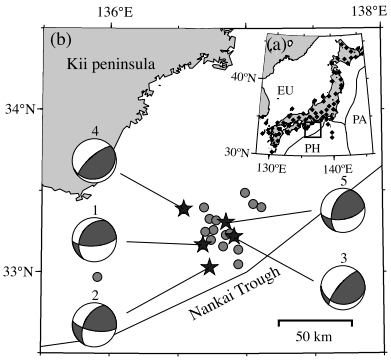

Figure 1. (a) Tectonic setting and location of NIED F-net seismic stations. Solid diamond indicates the NIED F-net station; PH, the Philippine Sea Plate; EU, the Eurasian Plate; and PH, the Pacific Plate. (b) Epicentral distribution and focal mechanisms of the VLF earthquakes. Epicenters and focal mechanisms were obtained by the centroid moment tensor inversion method [*Ito and Obara*, 2006]. The solid star and circle indicate the epicenters of VLF earthquakes. The number with the focal mechanism denote the event ID shown in Table 1; their waveforms filtered with a pass band of 0.005–20 Hz show a slightly distinct phase of the P wave.

centroid time, suggesting that these were *P* or *S* wave phases.

[8] On the other hand, some observed waveforms that were filtered with pass bands of both 0.005–20 Hz and 0.01–0.1 Hz showed slightly distinct phases near the calculated arrival times of the *P* wave (Figure 2b). We calculated the Fourier spectrum amplitude for some parts of these phases at each station (Figure 3). The time window including the calculated *P* wave travel time was 21 s; it was unaffected by the phases of the *S* wave because we selected only those stations that showed a significant difference between the *P* wave and *S* wave travel times. For all the stations shown in Figure 2b, the amplitudes of the signal

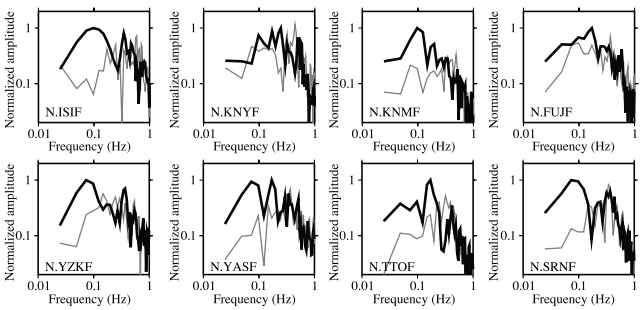

Figure 3. Fourier spectra of *P* waves at each station. All the spectra are calculated using a portion of the *P* wave arrival as shown in Figure 2b. The black and gray lines indicate the Fourier spectra of the *P* wave and the noise, respectively.

were larger than those of the noise at approximately 0.1 Hz. For five VLF earthquakes, we were able to detect the *P* wave signal at several stations (Table 1).

4. Spectral Analysis and Stress Drop

[9] In order to estimate the stress drop, we calculated the corner frequencies of a VLF earthquake using the shape of a stacked Fourier spectrum. The observed waveforms excited by the VLF earthquakes are well explained by a double-couple source [*Ito and Obara*, 2006]. Assuming an omega-square spectrum [*Boatwright*, 1978], we approximate the stacked velocity amplitude spectrum as

$$\bar{\tilde{u}}^{cal}(f) = C \cdot \frac{f}{\left(1 + (f/f_c)^4\right)^{1/2}} \cdot \exp\left(-\frac{\pi f \bar{t}^p}{Q^p}\right), \qquad (1)$$

where f_c, $\bar{t}^p$, and Q^p are the corner frequency, average travel time, and attenuation coefficient of the *P* wave, respectively. The constant *C* is related to the seismic moment, radiation pattern, and geometrical spreading effect. We used $\bar{t}^p$ = 40

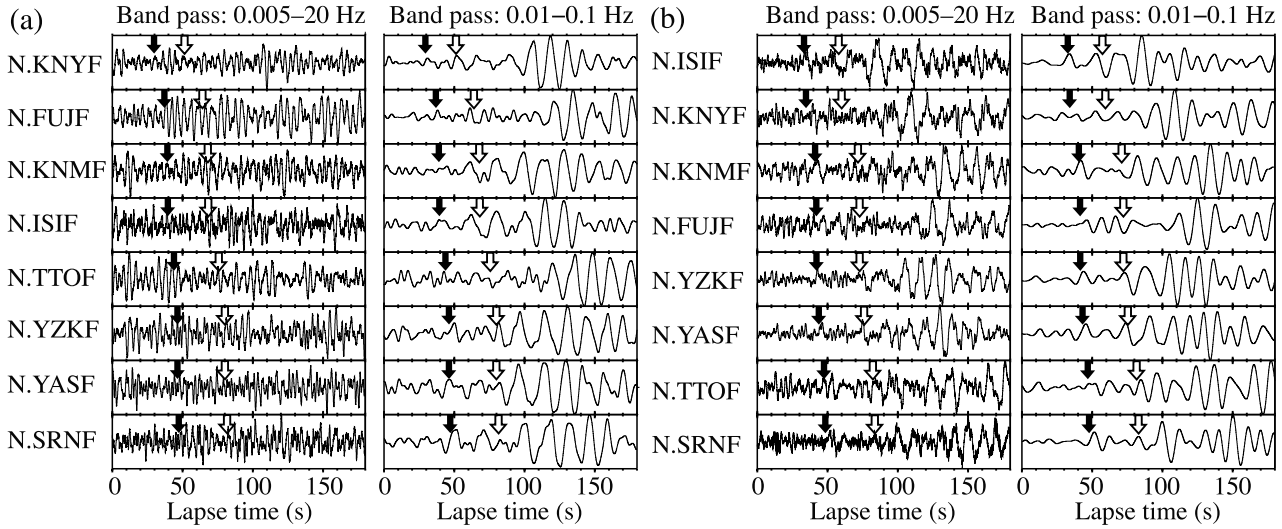

Figure 2. Two examples of waveforms for VLF earthquakes. (a) Waveforms with no distinct short period phase of the *P* wave. (b) Waveforms with a slightly distinct phase of the *P* wave. The solid and open arrows indicate the calculated *P* wave and *S* wave arrival time for each VLF earthquake, respectively.

Table 1. Source Parameters of the VLF Earthquakes Observed for a Slightly Distinct *P* Wave

ID	Centroid Time, UT	Lat, °N	Lon, °E	Depth, km	Mw	Moment, Nm	*fc*, Hz	Stress Drop, kPa
1	2004/09/12 16:44:17	33.17	136.68	2	3.8	5.517×10^{14}	0.11	0.1–0.8
2	2004/09/16 15:35:21	33.03	136.73	3	3.9	1.029×10^{15}	0.08	0.07–0.6
3	2004/09/18 04:17:59	33.22	136.91	4	3.9	8.406×10^{14}	0.18	0.6–5
4	2004/09/20 05:18:38	33.39	136.54	3	4.1	1.569×10^{15}	0.10	0.2–2
5	2004/09/20 05:59:27	33.31	136.85	2	3.7	3.841×10^{14}	0.24	0.7–6

because only the *P* wave spectra obtained at the stations with a travel time of 30–50 s were stacked. According to the relationship between the frequency and the attenuation factor of the *P* wave compiled by *Sato and Fehler* [1998], the latter shows a small frequency dependence with a magnitude of approximately 100. Using $\bar{t}^P = 40$ and $Q^P = 100$, we find the most suitable corner frequency f_c and constant C from the stacked Fourier spectrum by a grid search that minimizes the following residual:

$$Res = \int \left(\log \bar{u}^{cal}(f) - \bar{u}^{obs}(f)\right)^2 df, \tag{2}$$

where $\bar{u}^{obs}(f)$ is the stacked observed Fourier spectrum.

[10] Assuming a circular crack, we calculate the stress drop by *Brune* [1970] using

$$\Delta\sigma = \frac{7}{16} M_o \left(\frac{2\pi f_c}{2.34 V_p}\right)^3, \tag{3}$$

where V_p and M_o are the velocity of the *P* wave and the seismic moment, respectively. We used the seismic moments calculated by the centroid moment tensor inversion method [*Ito and Obara*, 2006]; these are shown in Table 1. Most of the VLF earthquakes occurred within a shallow portion of the sedimentary wedge of the accretionary prism between the trough axis and the outer ridge, which has a *P* wave velocity of 2–4 km/s [*Nakanishi et al.*, 2002]. Assuming that the *P* wave velocity of the accretionary prism is 2.0 and 4.0 km/s, we calculated the stress drop for these two cases and estimated the possible width of the two calculated stress drops for each VLF earthquake.

[11] Figure 4 shows an example of the spectral analysis for a VLF earthquake with a moment magnitude of 4.1; this is one of the largest events occurring off the Kii peninsula. The estimated corner frequency and stress drop were 0.10 Hz and 0.2–2 kPa, respectively. The synthetic spectrums were in good agreement with the stacked ones. Other estimations are shown in Table 1. The estimated stress drops of five VLF earthquakes were approximately 0.1%–1% of those of ordinary earthquakes, which show a stress drop of 1–10 MPa [e.g., *Kanamori and Anderson*, 1975].

5. Discussion

[12] VLF earthquakes are located between the deformation front and the outer ridge within accretionary prisms; they exhibit reverse faulting and, in particular, are associated with the dynamic deformation of the accretionary prism [*Ito and Obara*, 2006]. The seismic profile revealed well-developed out-of-sequence thrusts (OSTs) that branch from the decollement [*Moore et al.*, 1990], and mega-splay faults branched from the megathrust on the plate boundary [*Park et al.*, 2002]. Therefore, the VLF earthquakes probably occur along the OSTs or mega-splay faults due to the shortening of the accretionary prism. These thrust faults generate a reverse-polarity reflection on the seismic reflection profiles, indicating either the existence of elevated fluid pressures within the fault zones [*Shipley et al.*, 1994] or the fault zones being pathways of fluid migration [*Park et al.*, 2002] in the subduction zone. A possible fault model for explaining a very low stress-drop earthquake within the accretionary prism is as follows: High fluid pressure weakens the fault strength of the OST and mega-splay faults through a reduction in the normal stress on the fault plane; the resulting stick-slip behavior produces extremely low stress-drop faulting.

[13] We estimated the fault radius and slip of the largest VLF earthquake, as listed in Table 1, which was located the farthest from the Nankai Trough at the well-developed accretionary prism. Figure 5 shows the relationship between the fault radius and the size of the dislocation for the earthquake with a moment magnitude of 4.1; in this case, we used the abovementioned *P* wave velocities of 2 and 4 km/s. Further, we used a density ρ of 2300 kg/m^3 from the results obtained by the Ocean Drilling Program at the accretionary prism off southwestern Japan (Site 808) [*Davis et al.*, 2006]. Poisson's ratio within the accretionary prism was estimated by *Takahashi et al.* [2002], and we adopted a Poisson's ratio of 0.4, i.e., $V_p/V_s = 2.4$. For an ordinary earthquake with a moment magnitude of 4.1, the estimated fault radius was empirically estimated as approximately 0.5–1 km [e.g., *Utsu*, 2001]. Using the relationship between the fault radius and stress drop, $\Delta\sigma \propto 1/r^3$, and the result that the stress drop of a VLF earthquake is approximately

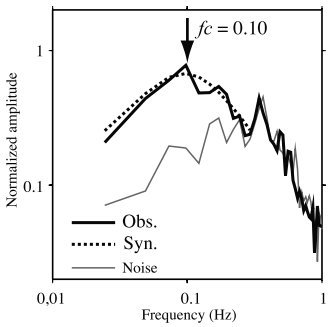

Figure 4. Example of spectral analysis for a *P* wave of the VLF earthquake. The black solid and gray lines indicate the stacked Fourier spectra of the *P* wave and the noise, respectively. The dotted line indicates the synthetic spectrum. The estimated corner frequency for this event is shown by an arrow.

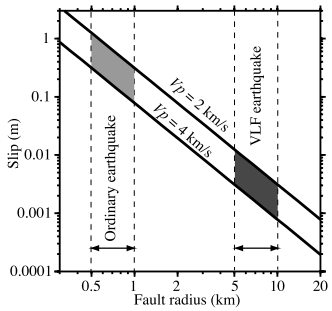

Figure 5. Relationship between the fault radius and slip for the largest VLF earthquake. See the text for details.

0.1% of an ordinary earthquake, we estimated the fault radius as 5–10 km, which was 10 times greater than the fault radius of an ordinary earthquake (Figure 5). We finally obtained a slip of 2–10 mm for the largest VLF earthquake. Using $V_s = V_p/2.4$ and $V_p = 2\sim 4$ km/s, we obtained the rupture velocity $v = 0.8V_s = 0.67 \sim 1.3$ km/s. For this event, the width of the pulse of the *P* wave is approximately 10 s, which was considered as the rupture duration *T* (Figure 2b). Moreover, using the rigidity $\mu = V_s^2\rho = 1600 \sim 6400$ MPa and the effective stress $\sigma_{eff} \approx \Delta\sigma = 200 \sim 2000$ Pa, we calculated the slip velocity $\dot{u} = 2V_s\sigma_{eff}/\mu$ [*Brune*, 1970] and obtained $\dot{u} = 0.05 \sim 2$ mm/s. A rise time τ of approximately 5 s is also estimated from Figure 2b. The estimated rupture velocity and slip velocity are lower than those of ordinary earthquakes, and the fault size and slip estimated by the products of v and T and τ and $\dot{u}$ are approximately consistent with those shown in Figure 5.

[14] Considering that the thickness of the accretionary prism off the Kii peninsula is limited to 5–10 km [*Nakanishi et al.*, 2002], it is possible that the largest magnitude of the VLF earthquakes occurring off the Kii peninsula is potentially restricted to approximately 4. In other words, the largest magnitude of the VLF earthquakes might be controlled by the thickness of the accretionary prism.

6. Conclusion

[15] We investigated the seismograms of the VLF earthquakes that occurred within the accretionary prism along the Nankai Trough, Japan. *P* waves composed of a wave train with a dominant period of approximately 10 s were discovered for some of the VLF earthquakes. We also calculated their stress drops by calculating the corner frequencies of the *P* waves; they were estimated as 0.1–10 kPa, which corresponds to 0.1%–1% of those of ordinary earthquakes. We estimated the possible fault radius and slip for one of the largest VLF earthquakes with a slightly distinct *P* wave phase. The maximum fault size and slip were estimated as approximately 10 km and 10 mm, respectively.

[16] **Acknowledgments.** The article was significantly improved through constructive reviews by Gregory C. Beroza and Gregory F. Moore. The generic mapping tools (GMT) software [*Wessel and Smith*, 1991] was used to prepare the figures.

References

Boatwright, J. (1978), Detailed spectral analysis of two small New York State earthquakes, *Bull. Seismol. Soc. Am.*, *68*, 1131–1177.

Brune, J. N. (1970), Tectonic stress and spectra of seismic shear waves from earthquakes, *J. Geophys. Res.*, *75*, 4997–5009. (Correction, *J. Geophys. Res.*, *76*, 5002, 1971).

Davis, E. E., K. Becker, K. Wang, K. Obara, Y. Ito, and M. Kinoshita (2006), A discrete episode of seismic and aseismic deformation of the Nankai Trough subduction zone accretionary prism and incoming Philippine Sea plate, *Earth Planet. Sci. Lett.*, *242*, 73–84.

Ito, Y., and K. Obara (2006), Dynamic deformation of the accretionary prism excites very low frequency earthquakes, *Geophys. Res. Lett.*, *33*, L02312, doi:10.1029/2005GL024711.

Kanamori, H., and D. L. Anderson (1975), Theoretical basis of some empirical relations in seismology, *Bull. Seismol. Soc. Am.*, *65*, 1073–1095.

Moore, G. F., T. H. Shipley, P. L. Stoffa, D. E. Karig, A. Taira, S. Kuramoto, H. Tokuyama, and K. Syuehiro (1990), Structure of the Nankai Trough accretionary zone from multichannel seismic reflection data, *J. Geophys. Res.*, *98*, 8753–8765.

Nakanishi, A., N. Takahashi, J. O. Park, S. Miura, S. Kodaira, Y. Kaneda, N. Hirata, T. Iwasaki, and M. Nakamura (2002), Crustal structure across the coseismic rupture zone of the 1994 Tonankai earthquake, the central Nankai Trough seismogenic zone, *J. Geophys. Res.*, *107*(B1), 2007, doi:10.1029/2001JB000424.

Obara, K. (2002), Nonvolcanic deep tremor associated with subduction in southwest Japan, *Science*, *296*, 1679–1681.

Obara, K., and Y. Ito (2005), Very low frequency earthquake excited by the 2004 off the Kii peninsula earthquake: A dynamic deformation process in the large accretionary prism, *Earth Planets Space*, *57*, 321–326.

Obara, K., H. Hirose, F. Yamamizu, and K. Kasahara (2004), Episodic slow slip events accompanied by non-volcanic tremors in southwest Japan subduction zone, *Geophys. Res. Lett.*, *31*, L23602, doi:10.1029/2004GL020848.

Kasahara, Y., K. Hori, S. Obara, K. Sekiguchi, S. Fujiwara, and H. Yamamoto (2004), Recent progress of seismic observation networks in Japan—Hi-net, F-net, K-NET, and KiK-net—, *Earth Planets Space*, *56*, xv–xxvii.

Park, J. O., T. Tsuru, S. Kodaira, P. R. Cummins, and Y. Kaneda (2002), Splay fault branching along the Nankai subduction zone, *Science*, *297*, 1157–1160.

Sato, H., and M. C. Fehler (1998), *Seismic Wave Propagation and Scattering in the Heterogeneous Earth*, pp. 109–114, Springer, New York.

Seno, T., S. Stein, and A. E. Gripp (1993), A model for the motion of the Philippine Sea plate consistent with NUVEL-1 and geological data, *J. Geophys. Res.*, *98*, 17,941–17,848.

Shipley, T. H., G. F. Moore, N. L. Bangs, J. C. Moore, and P. L. Stoffa (1994), Seismically inferred dilatancy distribution, northern Barbados ridge decollement; Implications for fluid migration and fault strength, *Geology*, *22*, 411–414.

Takahashi, N., S. Kodaira, A. Nakanishi, J. O. Park, S. Miura, T. Tsuru, Y. Kaneda, K. Suyehiro, and H. Kinoshita (2002), Seismic structure of western end of the Nankai trough seismogenic zone, *J. Geophys. Res.*, *107*(B10), 2212, doi.10.1029/2000JB000121.

Utsu, T. (2001), *Encyclopedia of Earthquakes* (in Japanese), pp. 283–284, Asakura Syoten, Tokyo.

Wessel, P., and W. H. F. Smith (1991), Free software helps map and display data, *Eos Trans. AGU*, *72*, 445–446.

Y. Ito and K. Obara, National Research Institute for Earth Science and Disaster Prevention, Tenno-dai 3-1, Tsukuba 305-0006, Japan. (yito@bosai.go.jp)